Specia issue
Sci.Int.(Lahore),26(5).1811-1815,2014 ISSN 1013-5316; CODEN: SINTE 8

THE EFFECTS OF PIXEL AGGREGATION ON THE RADIOMETRIC PROPERTIES OF LANDSAT-8 SATELLITE IMAGERY

Muhammad Fahmi Razali[1], Asmala Ahmad[1], Nurul Iman Saiful Bahari[1], Othman Mohd[2]
[1]Department of Industrial Computing
[2]Department of System and Computer Communication
Faculty of Information and Communication Technology, Universiti Teknikal Malaysia Melaka, Hang Tuah Jaya, 76100 Durian Tunggal, Melaka
Email: m.fahmi.razali@gmail.com, asmala@utem.edu.my

ABSTRACT : *This study aims to evaluate the effects of pixel aggregation on the radiometric properties of Landsat-8 satellite imagery. Two images of north-western Peninsular Malaysia (i.e. clear day and cloudy day) were selected for the study. The aggregated average method was used due to its simplicity and practicality. Paired sample t-test and similarity matrix analysis were performed to assess and evaluate the effects of aggregation to Landsat-8 radiometric properties. The results show that the higher the aggregation scale the lower the similarity to the original pixel value for all bands. However, pixel aggregation does not significantly change the radiometric properties of all bands in both images except for the infrared bands in the clear image.*

KEYWORDS: Aggregation, Radiometric, Landsat-8, Satellite imagery, T-test, Similarity Matrix

1.0 INTRODUCTION

In remote sensing, pixel aggregation is commonly performed to facilitate processing of datasets with different spatial resolution recorded from multi-sensor sources. This is done prior to image mosaicking or image fusion since it is required that all pixels possess the same spatial resolution. Depending on applications, the outcome of pixel aggregation will then undergo subsequent processes such as segmentation, clustering [1], [2] and classification [3], [4]. In other words, pixel aggregation is a common resampling technique that resizes pixels in an image from fine to coarser resolutions.

During aggregation new pixel values are created to represent the finer pixels within the aggregated area [5]. Several methods have been used to calculate new values of aggregated pixels, which include the nearest neighbour (NN) and aggregated average (AA) method. The NN resampling is carried out by matching the nearest central pixel value of pixels within the aggregated area to the new pixel while AA resampling takes the arithmetic mean of pixels within the aggregated area.

[6] performed AA resampling on IKONOS imagery, from 4 m to 30 m resolution, prior to comparing its spectro-radiometric compatibility with Landsat-7 imagery at several sites in North America. [7] studied the scalability of normalised difference vegetation index (NDVI) derived from multiple sensors by using the AA resampling technique. [8] used the AA resampling to study the impact of different spatial resolution on the derivation of land surface temperature (LST) and urban heat island (UHI) in Madrid city.

Although AA is a more widely used resampling technique than NN, both aggregation processes may change the radiometric characteristics of the data. By aggregation, some spatial patterns could be highlighted; however, it may also cause information loss as a result from generalisation of spatial information [8]. Following this notion, it is imperative that these effects be evaluated quantitatively so that the error introduced by pixel aggregation can be understood.

Landsat-8 satellite is a newly launched Earth observing satellite to continue the missions of Landsat 5 and 7. It was launched on February 11, 2013 equipped with a 9-bands multispectral sensor or known as the operational land imager (OLI) and a 2-bands thermal sensor or known as thermal infrared sensor (TIRS) [9]. The sensors of Landsat-8 was design to closely resemble the spectral resolution of its predecessor, Landsat-7, to ensure compatibility with historical data while possessing additional 3 bands (deep blue and cirrus bands and splitting the thermal bands into two for improved Earth system observations. Figure 1 shows the atmospheric transmission and wavelengths for the Landsat-8 OLI and TIRS bands and Landsat-7 ETM+ bands [9].

The present article aims to measure the effects of AA resampling on images collected from Landsat-8 sensor. To avoid bias, two images of the same scene (clear and cloud day) will be used in the analyses. The clear day will represent noise-free data while cloudy day as noisy data.

2.0 METHODOLOGY

Two Landsat-8 images (path 128, row 56) of north-western Peninsular Malaysia on Feb 27th and May 2nd, 2014 were used in this study. The images cover part of Perlis, Kedah and Penang. Pre-processing was performed by geometrically correcting each image based on the West Malaysia RSO projection and calibrating Bands 1 to 7 and 9 to solar-angle corrected top-of-atmosphere reflectance and thermal Bands 10 and 11 to top-of-atmosphere radiance. Band 8 (panchromatic band) was excluded from this study. Table 1 shows Landsat-8 band specifications where bands 1 to 9 are OLI spectral bands while bands 10 and11 are TIRS spectral bands [9]. Figure 2 shows Landsat-8 band 6, 5 and 4 assigned to red, green and blue (RGB) for Feb 27th, 2014 (left) and May 2nd, 2014 (right) used in this study ENVI 4.5 software package was used where pixels

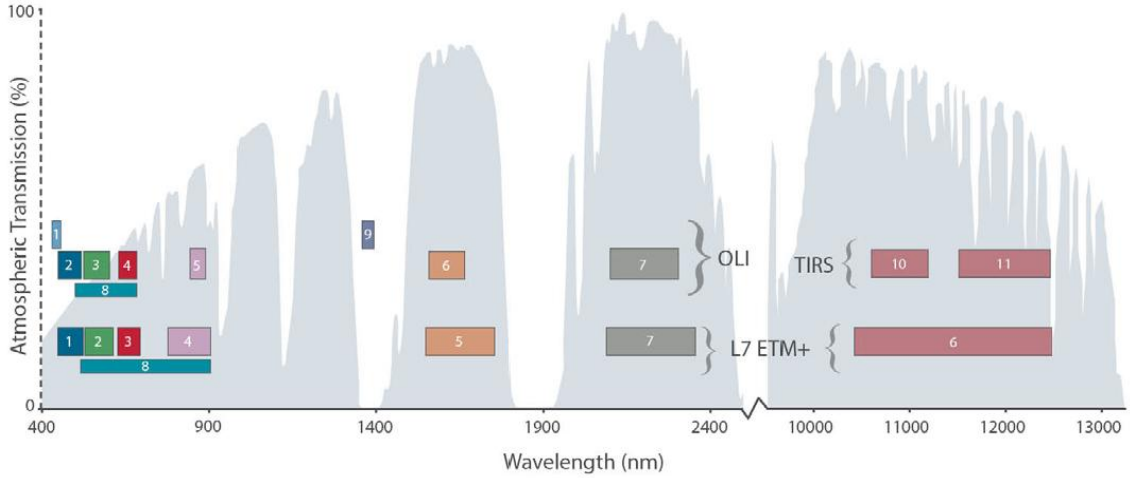

Figure 1: The spectral bands of Landsat-8 OLI and TIRS compared to Landsat-7 ETM+.

Table 1: Landsat-8 band specifications. Bands 1-9 are OLI spectral bands while bands 10-11 are TIRS spectral bands.

Spectral Band	Wavelength (μm)	Resolution (m)
Band 1 - Coastal / Aerosol	0.433 - 0.453	30
Band 2 - Blue	0.450 - 0.515	30
Band 3 - Green	0.525 - 0.600	30
Band 4 - Red	0.630 - 0.680	30
Band 5 - Near Infrared (NIR)	0.845 - 0.885	30
Band 6 - Short Wavelength Infrared (SWIR)	1.560 - 1.660	30
Band 7 - Short Wavelength Infrared (SWIR)	2.100 - 2.300	30
Band 8 - Panchromatic	0.500 - 0.680	15
Band 9 - Cirrus	1.360 - 1.390	30
Band 10 - Long Wavelength Infrared	10.30 - 11.30	100
Band 11 - Long Wavelength Infrared	11.50 - 12.50	100

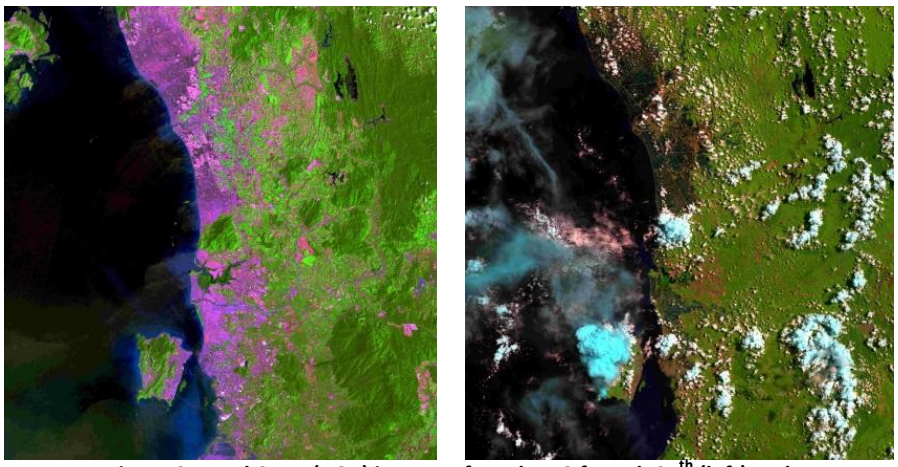

Figure 2: Band 6-5-4 (RGB) images of Landsat-8 for Feb 27th (left) and May 2nd, 2014 (right) used in this study.

Table 2: Significance table from the paired sample t-test of clear day image. Results with only significant effects are presented (p<0.05).

	Paired sample (resolution, m^2)			
	30 m^2 – 120 m^2	30 m^2 – 250 m^2	30 m^2 – 500 m^2	30 m^2 - 1000 m^2
Band 5 (NIR)	0.002	0.002	0.003	0.004
Band 6 (SWIR 1)	0.007	0.002	0.007	0.002
Band 7 (SWIR 2)	0.046	0.018	0.035	0.005

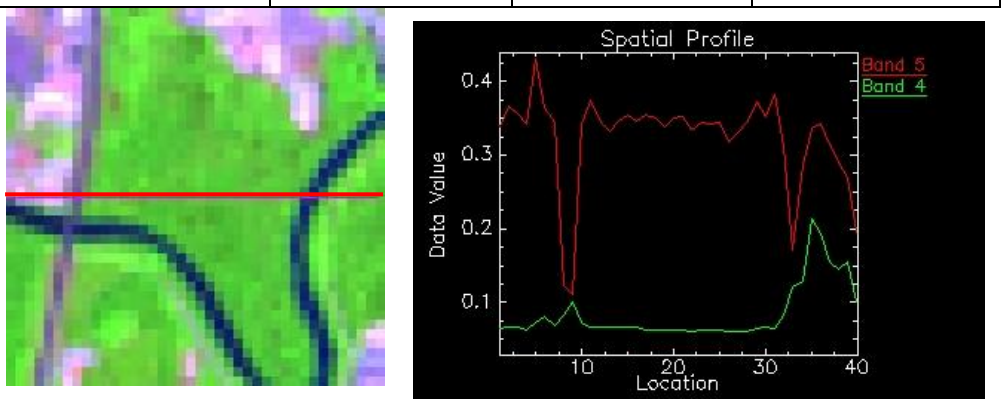

Figure 3: Clear day image subsetted from Figure 2 (left) and spectral profile of band 4 and 5 from red transect (right).

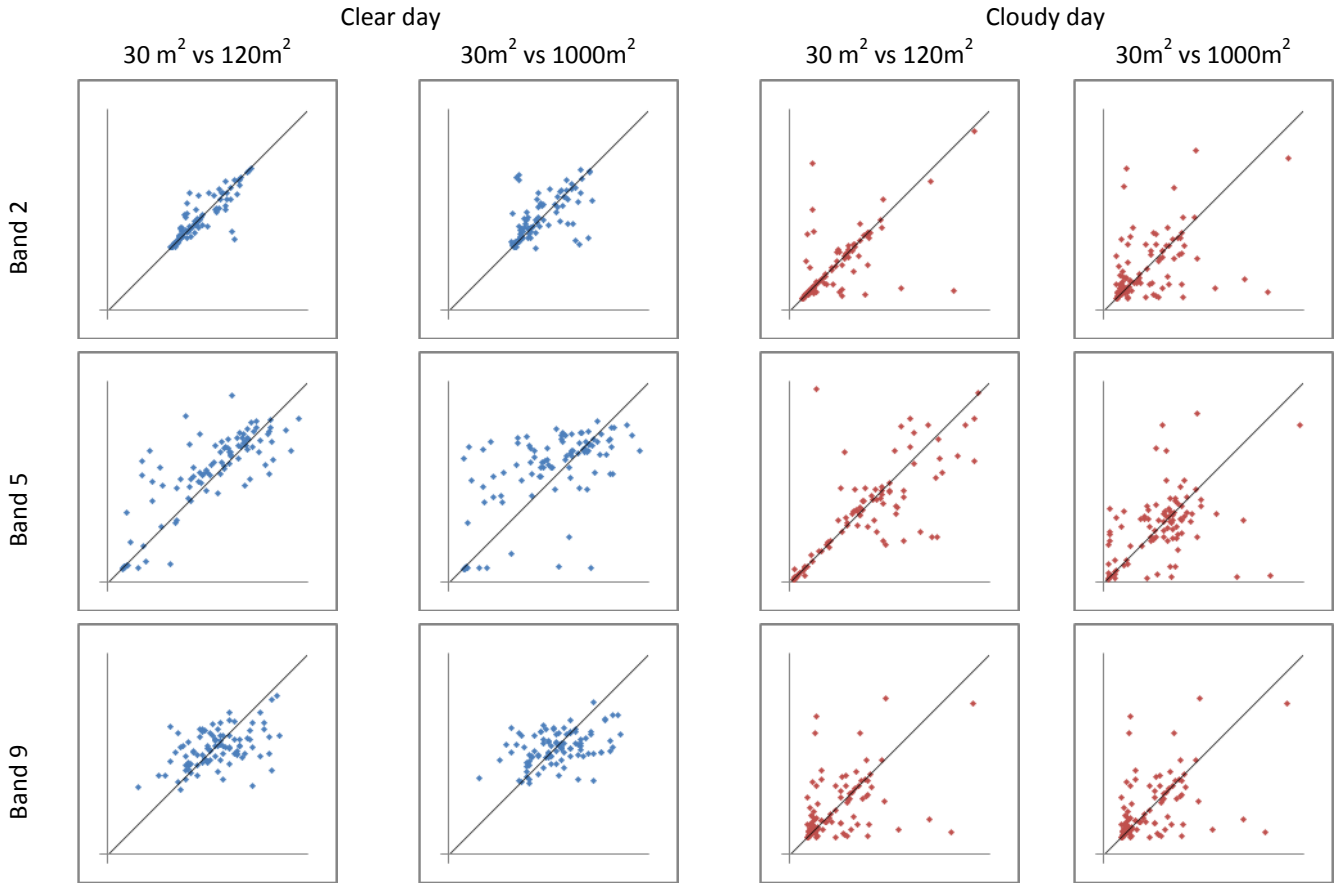

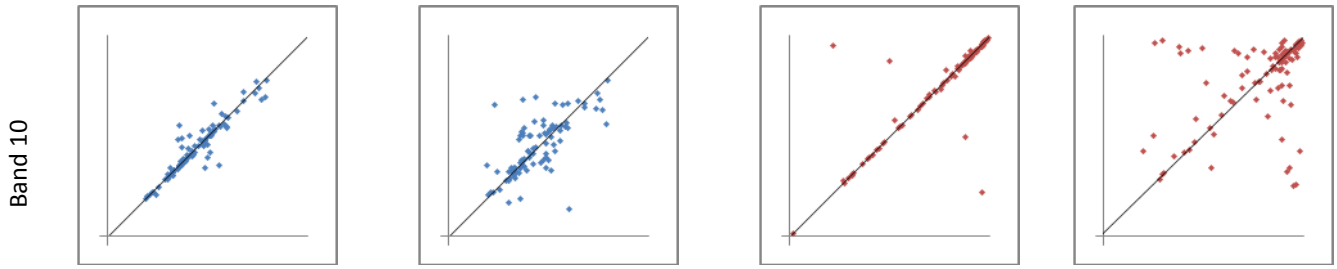

Figure 4: Scatterplots for clear (blue) and cloudy (red) day images. The diagonal line represents the *y=x*.

Table 2: Similarity matrix between original and aggregated resolutions for all bands and for clear and cloudy images.

	Clear day				Cloudy day			
	120	250 m^2	500	1000	120 m^2	250	500 m^2	1000
Band 1	0.90	0.765	0.70	0.65	0.662	0.70	0.655	0.44
Band 2	0.88	0.746	0.68	0.63	0.657	0.69	0.650	0.44
Band 3	0.83	0.721	0.62	0.53	0.672	0.70	0.665	0.46
Band 4	0.67	0.646	0.52	0.51	0.659	0.69	0.659	0.44
Band 5	0.81	0.755	0.69	0.60	0.691	0.75	0.678	0.48
Band 6	0.80	0.774	0.61	0.55	0.640	0.73	0.570	0.47
Band 7	0.79	0.738	0.57	0.59	0.614	0.70	0.581	0.45
Band 9	0.45	0.479	0.37	0.39	0.744	0.79	0.666	0.57
Band 10	0.93	0.843	0.61	0.70	0.861	0.84	0.610	0.50
Band 11	0.93	0.847	0.61	0.71	0.856	0.84	0.637	0.51

Resampling was carried out using the AA pixel aggregation method. In this study, both images were resampled from the original
30 m^2 to 120 m^2, 250 m^2, 500 m^2 and 1000 m^2 resolution. From the generated images, 100 pixels were randomly sampled and compared to the pixel values of the respective original images. Comparisons were facilitated by paired sample t-test, and similarity matrix using the Pearson correlation coefficient (R) between all possible combinations, i.e. 30 m^2 – 120 m^2, 30 m^2 – 250 m^2, 30 m^2 – 500 m^2 and 30 m^2 – 1000 m^2.

3.0 RESULTS AND DISCUSSION

Results from the t-test shows that all aggregation of Landsat-8 pixel up to 1000 m^2 resolution did not significantly change the overall radiometric properties for both images. However all the reflective IR bands in the clear image (bands 5, 6 and 7) were the only bands to experience a significant change ($p<0.05$) in reflectance value when aggregated to all designated resolution (Table 2). Further spectral analysis revealed that the reflective IR bands of Landsat-8 are very sensitive to different land covers and different pixel of the same land cover type than the visible reflective bands. Figure 3 shows an example of Band 5 (NIR band) fluctuating more within land cover pixels compared to Band 4 (red band). Since the random sampling of pixels also selected pixels in heterogeneous land cover areas, it is possible that during aggregation pixel radiometric values (especially the reflective IR bands) are affected. Work by 0 and [7] also found aggregation over heterogeneous land covers led to significant change in radiometric values.
Although the radiometric properties of the reflective IR bands in the clear image have changed significantly when aggregated, it is still able to maintain similarities of approx. 50-80% of its original properties which are generally similar compared to the other bands (Table 2). However the similarities of Band 9 (cirrus band) in clear day were the lowest of all
bands (between 39-45%). Scatterplots in Figure 4 shows that most band 9 pixels are located away from the diagonal line meaning the radiometric properties are randomly changed after aggregation. Due to limited space only bands 2, 5, 9 and 10 are presented for 30m^2 against 120 and 1000m^2 relationships. Band 9 (cirrus band) of Landsat-8 is one of the newly introduced bands in the Landsat Mission series to improve detection of cirrus cloud contamination. Cirrus

clouds in general are difficult to detect compared to other cloud types due to its sparseness and irregular distribution. Hence it is possible that during aggregation pixels were average across cirrus free/contaminated pixels that are largely different in radiometric value.

Overall based on the similarity matrix (Table 2), all bands experience a noticeable decrease in similarity values when the aggregation scale is higher. The clear day image performs better at maintain its similarity compare to the cloudy image because of less contamination effects (noise) from clouds and cloud shadows which have high and low reflectance value respectively.

4.0 CONCLUSIONS

The effects of pixel aggregation on the radiometric properties of Landsat-8 reflective and thermal bands have been studied. The results suggest that aggregating pixels using the AA resampling technique can preserve the radiometric properties of all bands except the IR bands and cirrus band. The level of preservation depends on the aggregation scale, i.e. a lower aggregation scale can better preserve the radiometric properties than larger aggregation scales. Successfully identifying the effects of pixel aggregation can help users to understand and manage errors prior to further analyses.

ACKNOWLEDGEMENT

The authors would like to thank Universiti Teknikal Malaysia Melaka and Malaysian Ministry of Education for funding this study under the UTeM Short-term Research Grant (UTeM PJP) (No.: PJP/2013/FTMK(2B)/S01104).

REFERENCES

[1] A. Ahmad and S. Quegan. Comparative Analysis of Supervised and Unsupervised Classification on Multispectral Data. *Applied Mathematical Sciences*, vol. 7, no. 74, pp. 3681-3694, 2013.

[2] A. Ahmad. Analysis of Landsat 5 TM Data of Malaysian Land Covers Using ISODATA Clustering Technique. *Proceedings of the 2012 IEEE Asia-Pacific Conference on Applied Electromagnetics (APACE 2012)*, pp. 92-97, 2012.

[3] A. Ahmad. *Analysis of Maximum Likelihood Classification on Multispectral Data*, Applied Mathematical Sciences, vol. 6, no.129, pp. 280-285, 2012.

[4] A. Ahmad. Analysis of Maximum Likelihood Classification Technique on Landsat 5 TM Satellite Data of Tropical Land Covers. *Proceedings of 2012 IEEE International Conference on Control System, Computing and Engineering (ICCSCE2012)*. pp. 1-6, 2012.

[5] H. Studley and K. T. Weber. Comparison of Image Resampling Techniques for Satellite Imagery. In K. T. Weber & K. Davis, eds. *Final Report: Assessing Post-Fire Recovery of Sagebrush-Steppe Rangelands in Southeastern Idaho*. pp. 185–196, 2011.

[6] S. N. Goward, P. E. Davis, D. Fleming, L. Miller and J. R. Townshend. Empirical comparison of Landsat-7 and IKONOS multispectral measurements for selected Earth Observation System (EOS) validation sites. *Remote Sensing of Environment*, vol 88, pp. 80–99, 2003.

[7] J. Théau, T. Sankey and K. Weber. Multi-sensor analyses of vegetation indices in a semi-arid environment. *GIScience & Remote Sensing*, vol 47, no. 2, pp. 260–275, 2010.

[8] J. A.Sobrino, R. Oltra-Carrió, G. Sòria, R. Bianchi and M. Paganini. Impact of spatial resolution and satellite overpass time on evaluation of the surface urban heat island effects. *Remote Sensing of Environment*, vol 117, pp. 50–56, 2012.

[9] U.S. Geological Survey. *Landsat-8. USGS Fact Sheet*: 2013-3060, 2013.

[10] Z. Jiang, A.R. Huete, J. Chen, Y. Chen, J. Li, G. Yan and X. Zhang. Analysis of NDVI and scaled difference vegetation index retrievals of vegetation fraction. *Remote Sensing of Environment*, vol 101, pp. 366–378, 2006.